

Improved performance of Ag-doped TiO₂ synthesized by modified sol–gel method as photoanode of dye-sensitized solar cell

Arun Kumar Gupta¹ · Pankaj Srivastava¹ · Lal Bahadur¹

Received: 14 December 2015 / Accepted: 24 June 2016 / Published online: 8 July 2016
© Springer-Verlag Berlin Heidelberg 2016

Abstract Ag-doped TiO₂ with Ag content ranging from 1 to 7 mol% was synthesized by a modified sol–gel route, and its performance as the photoanode of dye-sensitized solar cells (DSSCs) was compared with undoped TiO₂ photoanode. Titanium(IV)isopropoxide was used as precursor and hexamethylenetetramine as the capping agent. XRD results show the formation of TiO₂ nanoparticles with an average crystallite size of 5 nm (1 % Ag-doped TiO₂) and 9 nm (undoped TiO₂), respectively. The TiO₂ nanopowder was used to prepare its thin film photoelectrode using doctor's blade method. Significant improvement in light-to-energy conversion efficiency was achieved when thin films of 1 % Ag-doped TiO₂ were applied as photoanode in DSSC taking N719 as the sensitizer dye. As evidenced by EIS measurements, the electron lifetime of DSSC with Ag-doped TiO₂ increased from 1.33 (for undoped TiO₂) to 2.05 ms. The short-circuit current density (J_{sc}), open-circuit voltage (V_{oc}), fill factor (FF) and the overall energy conversion efficiency (η) were 1.07 mA cm⁻², 0.72 V, 0.73 and 0.40 %, respectively, with the use of 1 % Ag-doped TiO₂ photoanode, whereas with undoped TiO₂ under similar conditions, $J_{sc} = 0.63$ mA cm⁻², $V_{oc} = 0.70$ V, fill factor 0.45 and conversion efficiency 0.14 % could be obtained. Therefore, compared with the reference DSSC containing an undoped TiO₂ photoanode, the power conversion efficiency of the cell based on Ag-doped TiO₂ has been remarkably enhanced by ~70 %. The substantial improvement in the device performance is attributed to the reduced band-gap energy,

retarded charge recombination and greater surface coverage of the sensitizing dye over Ag-doped TiO₂, which ultimately resulted in improved IPCE, J_{sc} and η values.

1 Introduction

Dye-sensitized solar cells (DSSCs) have emerged as an alternative to conventional silicon-based solar cells due to their relatively high energy conversion efficiency and low cost [1–3]. Semiconductors such as TiO₂ [4], ZnO [5], SnO₂ [6], Nb₂O₅ [7] and SrTiO₃ [8] have extensively been studied for use as photoanode materials to develop high-performance DSSCs. TiO₂ has been proven to be the best semiconductor electrode material due to its chemical stability, nontoxicity, good electrical properties and low cost, and therefore, it is widely used in many applications such as photocatalysis, hydrogen production and solar cells [9–12]. Sol–gel method is a fascinating method to synthesize TiO₂ due to its economical materials processing, high chemical purity, homogeneity and small particle size of the obtained TiO₂ [13]. Among anatase, rutile and brookite crystalline phases of titanium dioxide, anatase TiO₂ has the band-gap energy of 3.2 eV, for which the absorption thresholds correspond to 380 nm, suggesting for facile excitation under solar light irradiation. Nevertheless, properties of TiO₂ are severely limited as spectroscopic studies reveal that almost 90 % of the photogenerated electron–hole (e^-h^+) pairs recombine rapidly after excitation. Researches have focused on improving performance by modifying its surface by deposition of noble metals, thus extending absorption spectrum toward the visible region. Pt, Au, Ag, Cu have been largely doped in TiO₂ to improve its properties. The dopant ions contribute to the change of electronic structure and light absorption

✉ Pankaj Srivastava
pankaj_bhuin@rediffmail.com

¹ Department of Chemistry, Institute of Science, Banaras Hindu University, Varanasi 221005, India

efficiency of the TiO₂. Specially, noble metals like Au and Ag have electron storage properties, thus facilitating charge separation in semiconductor–metal composites [14].

Many reports are there in which Ag-doped TiO₂ has been employed as photoanode for DSSC application because it is comparatively cheap and the work function of silver is greater than Fermi level of TiO₂ leading to effective tuning of the band gap. Chang et al. [15] have shown that Ag at TiO₂ photoanode forms a porous structure, which possesses not only great surface area, but also good adsorption of dye could be achieved, and DSSC employing such a photoanode showed a photoelectric conversion efficiency of 6.06 % with controlled thickness of the film. Huang et al. [16] observed an improved interfacial electron transfer and light harvesting in dye-sensitized solar cells by using Ag nanowire/TiO₂ nanoparticle composite films. The energy conversion efficiency of the DSSC with AgNWs reached 5.31 % compared to 4.68 % for DSSC without AgNWs. Dissanayak et al. [17] have shown that the efficiencies of plasmonic DSSCs with TiO₂:AgNP were 6.51 %, representing an efficiency enhancement by 27 % for AgNPs, and ascribed it to localized surface plasmon resonance effect narrowing the energy band gap of TiO₂ due to the presence of Ag nanoparticles. Yunyu et al. [18] have ascribed similar observations to enhanced conductivity of TiO₂ thin-film photoanode, causing fast electron transport and correspondingly an increase in photocurrent. Jin et al. [19] reported that the electron lifetime of DSSCs with Ag-doped TiO₂ nanofiber increased from 0.29 to 0.34 s and that electron recombination was reduced, and as a consequence, the conversion efficiency of TiO₂ photoelectrode-based DSSCs was increased from 4.74 to 6.13 % after adding 5 wt% ATN into TiO₂ films. Huang et al. [20] reported that the enhancement of light trapping (which leads to the increase in photocurrent), increase in open-circuit voltage and reduction of charge transport resistance led to the improvement of cell efficiency when thermally shrunk Ag nanoparticles were used as the etching masks for nanoporous TiO₂ photoanodes.

The incorporation of Ag nanoparticles is beneficial for promoting the charge separation within the TiO₂ film as well as improves the interfacial charge-transfer process. This results in an enhanced electrical conductivity [21]. In fact, electron transport in the DSSCs is dominated by diffusion and a faster electron transport results in a higher photocurrent. Li et al. [22] reported that the electron diffusion coefficient of the Ag-doped DSSC is about three times higher as compared to the undoped DSSC. Additionally, silver incorporated on TiO₂ could be attributed to accelerate the formation of superoxide radical anion O²⁻ and also decrease the probability of recombination of electrons and holes by scavenging the electrons in the

conduction band by silver dopants. Doping the TiO₂ with silver ions (Ag⁺ and Ag²⁺) may lead to the formation of space charge, and the e^-/h^+ pairs are efficiently separated by the large electric field before recombination [23]. Moreover, since the work function of silver is greater than Fermi level of TiO₂, when they are in contact, a Schottky barrier is created, which facilitates the transfer of photo-generated electrons from TiO₂ to Ag NPs and retards the recombination of electron–hole pairs [24]. The another merit of Ag/TiO₂ composites, which the light absorption spectrum is extended toward the visible region, can be ascribed to the effect of Ag by acting as electron traps in TiO₂ band gap [23].

In this work, we have synthesized undoped and Ag-doped TiO₂ by a modified sol–gel method making use of hexamethylenetetramine (HMT) as capping agent and applied as the photoanode material in DSSC. The prime focus was to substantiate the idea that with the additive effect of capping agent and dopant, there is possibility of additional enhancement of sensitized photocurrent. The crystal structure of TiO₂ and Ag-loaded TiO₂ was examined by XRD. Morphologies and particle sizes of TiO₂ and Ag-loaded TiO₂ were investigated by SEM, HR-TEM and AFM. The chemical composition of TiO₂ and Ag-loaded TiO₂ nanoparticles was examined by EDXS. Photovoltaic performance was studied in DSSC configuration employing N719 dye.

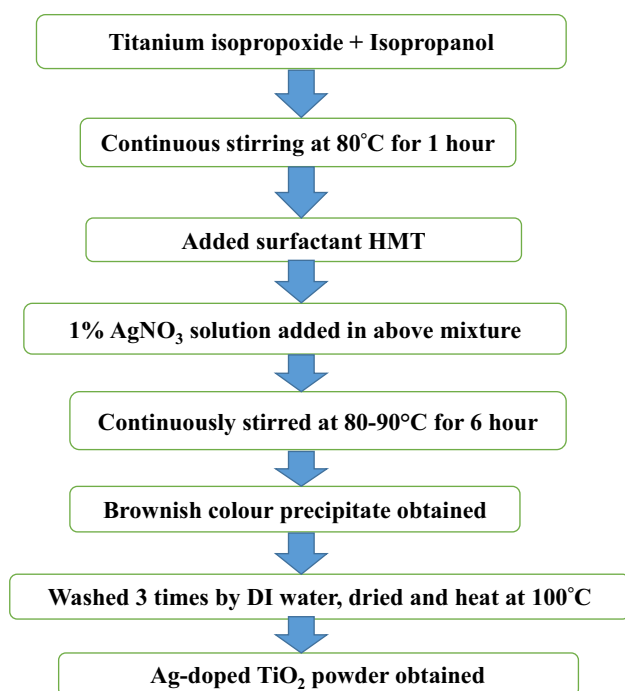
2 Experimental

2.1 Materials

Titanium(IV)isopropoxide (Sigma-Aldrich), silver nitrate (Merck), isopropanol (Merck) and hexamethylenetetramine, HMT (Merck, purity >99 %) were used as received for preparing TiO₂ powders. LiI (99.9 %, Aldrich), I₂ (G. R. grade, 99.8 %, BDH) added as redox couple in cell electrolyte and propylene carbonate (>99 %, Merck) taken as the medium of cell electrolyte were used without any further purification. Platinum catalyst (T/SP paste) used for making counter electrode, the sealing agent (SX1170-60, 50 μm) and N719 dye used as photosensitizer were all obtained from Solaronix SA. Conducting glass plate (15 Ω/sq) was obtained from Pilkington, USA.

2.2 Preparation of TiO₂ powder

Undoped TiO₂ and Ag-doped TiO₂ were synthesized by sol–gel method as detailed in Scheme 1. 0.2 M solution of titanium isopropoxide was prepared in isopropanol with constant stirring for 1 h. Then, 0.2 M hexamethylenetetramine was added into the above solution dropwise with



Scheme 1 Synthesis procedure of preparing undoped and Ag-doped TiO₂

constant stirring for another 1 h. For preparing the Ag-doped samples, AgNO₃ solution was mixed in above solution dropwise, and the final mixture was then refluxed for 6 h at 80 °C to get clear solution. The brownish-white precipitate (in case silver-doped samples) and white precipitate in case of undoped TiO₂ were obtained. The resulting precipitates were filtered and washed with distilled water followed by ethanol and dried at 100 °C. Finally, the TiO₂ powders were annealed at 450 °C for 1 h.

2.3 Material characterization

The absorption and FTIR spectra of doped and undoped TiO₂ powders were recorded with Shimadzu UV-1700 spectrophotometer and Varian 3100 FT-IR spectrometer, respectively. X-ray diffraction (XRD) study of the samples was carried out using D8 Advance X-ray diffractometer equipped with graphite monochromator and a Cu source ($\lambda = 1 \times 5418 \text{ \AA}$, CuK α operating at 45 kV and 40 mA). AFM images were recorded by NT-MDT atomic force microscope (model Solver NEXT). Roughness was reckoned by NOVA Px 3.1.0 software. EIS studies were carried out using Autolab electrochemical workstation (model AUT 302 N). SEM and EDAX were obtained using SEM EVO Scanning Electron Microscope MA 15/18 and EDAX EDS 51N1000, respectively. HRTEM was carried out using HRTEM, TECNAI 20G² (200kv) FEI company, Netherland.

2.4 Preparation of TiO₂ electrode (photoanode) and counter electrode

TiO₂ thin-film electrodes (photoanodes) were prepared by spreading the paste of as-synthesized TiO₂ powders (prepared with ethanol) on the fluorine-doped tin oxide (FTO) glass substrates and applying the doctor's blade method. Films were dried under ambient condition and annealed at 450 °C in air for 1 h in a tubular furnace. This resulted in TiO₂ film of $\sim 6 \mu\text{m}$ thickness. The dye (N719) was anchored onto the surface of the TiO₂ thin film electrode by immersing it into ethanol solution of dye for 18 h. The platinum counter electrode was prepared on another FTO-coated glass substrate by depositing platinum catalyst using doctor's blade method and annealing at 400 °C for half an hour in air.

2.5 Fabrication of DSSC

The photoelectrode (dye-coated TiO₂ film) was put over platinum counter electrode in such a way that the conductive side of both the electrodes faced each other, and the cell was sealed from three sides using spacer/sealing tape (heating it at $\sim 80 \text{ }^\circ\text{C}$); one side was left open for the injection of electrolyte. The cell electrolyte (0.2 M lithium iodide and 0.02 M iodine in propylene carbonate) was injected through open side and was drawn into the space between the electrodes by capillary action. Thereafter, the open side of the cell assembly was sealed properly with araldite, and the contacts were made by copper wires using silver paste.

2.6 Photoelectrochemical measurements

A bi-potentiostat (Model no. AFRDE 4E, Pine Instrument Company, USA) and e-corder (Model 201, eDAQ, Australia) were used for current–potential measurements. For photoelectrochemical (PEC) measurements, a 150-W Xenon arc lamp with lamp housing (Model no. 66057) and power supply (Model no. 68752), all from Oriel Corporation, USA, were used as the light source. The semiconductor electrode was illuminated after passing the collimated light beam through a 6-inch-long water column (to filter IR part of the light) and condensing it with the help of fused silica lenses (Oriel Corporation, USA). The UV part of this IR-filtered light was cut off by using a long-pass filter (Model no. 51280, Oriel Corporation, USA), and the light obtained this way was used for irradiation. To obtain the action spectrum ($J_{\text{photo}}-\lambda$) of the dye-sensitized TiO₂ electrode, monochromatic light-induced photocurrent was measured with the help of a digital multimeter (Philips Model No. 2525) in combination with the potentiostat. The light was monochromatized, by using a grating

monochromator (Oriel Model 77250 equipped with model 7798 grating). The width of the exit slit of the monochromator was kept at 0.5 mm. The intensities of light were measured with a digital photometer (Tektronix model J16 with model J 6502 sensor).

3 Results and discussion

3.1 Material characterizations

3.1.1 Optical properties of undoped and Ag-doped TiO₂

Figure 1 shows the absorption spectra of the undoped and 1 % Ag-doped TiO₂ powders. From the figure, it is evident that the undoped TiO₂ shows absorption in UV region only, whereas 1 % Ag-doped TiO₂ shows appreciable absorption in the visible region of solar spectrum. This clearly indicates that the Ag doping has effectively extended the spectral sensitivity of TiO₂ in the visible region. The band gap(s) of the undoped and 1 % Ag-doped TiO₂ were obtained using the following relation:

$$(\alpha h\nu)^{1/2} = B(h\nu - E_g) \quad (1)$$

where B is a constant, E_g the band gap of the material, α is the absorption coefficient (cm^{-1}) and $h\nu$ is the photon energy. Based on this equation, the optical band gap (E_g) of the TiO₂ was obtained by extrapolating the linear portion of $[(\alpha h\nu)^{1/2}$ vs $h\nu]$ plot to $\alpha \rightarrow 0$ as shown in Fig. 2. The results obtained have shown that the band gap became narrower and red-shifted for Ag-doped TiO₂ (3.10 eV for the undoped TiO₂ to 2.75 eV for 1 % Ag-doped TiO₂). The narrower band gap is in fact due to a downward shift in the conduction band and upward shift in the valence band,

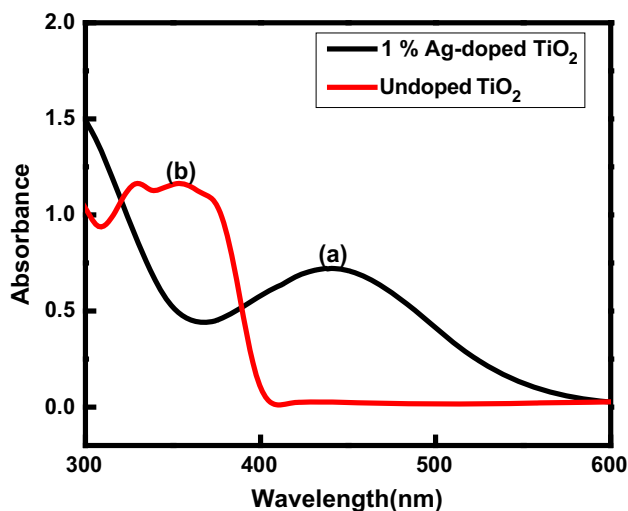


Fig. 1 UV-Vis spectra of a undoped TiO₂ and b 1 % Ag-doped TiO₂

which leads to a decrease in the band gap. It facilitates better conduction of electrons under illumination, and therefore, improved light-harvesting properties of Ag-doped TiO₂ electrodes compared to undoped TiO₂ are anticipated.

3.1.2 FTIR spectra

The FTIR spectra of undoped and 1 % Ag-doped TiO₂ recorded in the range of 4000–400 cm^{-1} are shown in Fig. 3. It was observed that undoped and 1 % Ag-doped TiO₂ samples exhibited quite similar FTIR spectra. An examination of the spectra reveals the peaks in the range of 400–900 cm^{-1} , which are characteristics of the formation of O–Ti–O lattice and Ti–O stretching mode [25]. The

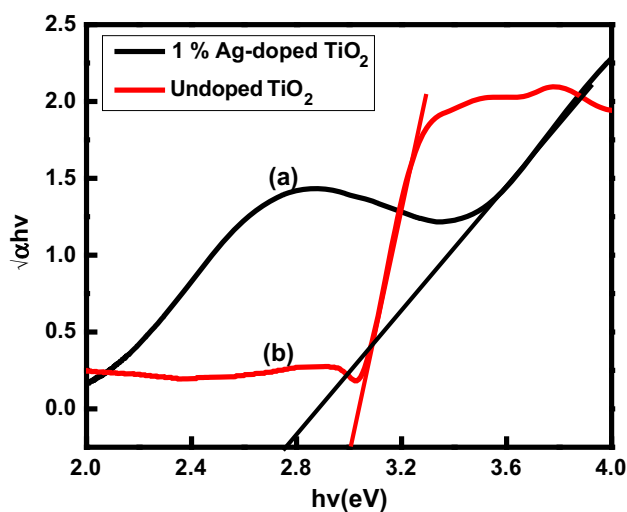


Fig. 2 Band-gap determination of a undoped TiO₂ and b 1 % Ag-doped TiO₂

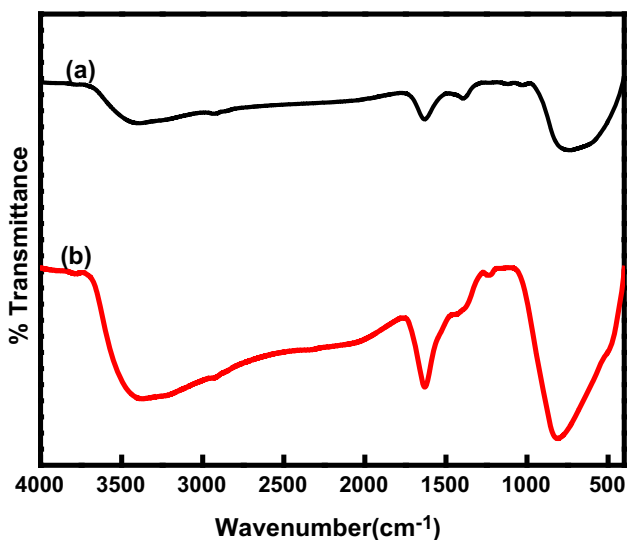


Fig. 3 FTIR spectra of a 1 % Ag-doped TiO₂ and b undoped TiO₂

peak around $\sim 1630\text{ cm}^{-1}$ corresponds to bending vibration of H–O bond [26]. The broadband observed at $2900\text{--}3400\text{ cm}^{-1}$ may be assigned to the stretching vibration of –OH and weakly bound water molecules [27, 28].

3.1.3 X-ray diffraction

The doping of Ag in the TiO₂ lattice was confirmed by X-ray powder diffraction (XRD). Figure 4 shows the XRD spectra for the undoped and 1 % Ag-doped TiO₂ powders. Its comparison with the JCPDS Card File No. 21-1272 has proven that XRD patterns for all the samples have anatase structure. The diffraction peaks that appeared at 25.3° , 37.8° , 48.1° , 54.0° , 54.9° and 62.7° (2θ values) have been assigned to $d(101)$, $d(004)$, $d(200)$, $d(105)$, $d(211)$ and $d(204)$ planes (of the anatase type structure), respectively. In fact, under the specific preparation conditions, the films are comprised of anatase only and rutile phase was not detected. From the broadening of X-ray diffraction peaks and using the Scherrer equation (Eq. 2), the crystallite size L has been estimated

$$L = K\lambda/\beta \cos \theta \quad (2)$$

K is a constant taken as 0.89, λ is the wavelength of the X-ray radiation (1.5418 \AA), β is the full width at half maximum height (FWHM) of the peak and θ is the diffracting angle. The average crystallite size of TiO₂ powders determined from strongest peak at 25.3° (101 plane) was found to be 5 nm (1 % Ag-doped TiO₂) and 9 nm (undoped TiO₂), respectively. The X-ray diffraction patterns of the silver-doped TiO₂ samples almost coincide with that of pure TiO₂ and show no diffraction peaks due to the silver species, thus suggesting that the metal particles are well dispersed on the TiO₂ surface. Doping with Ag

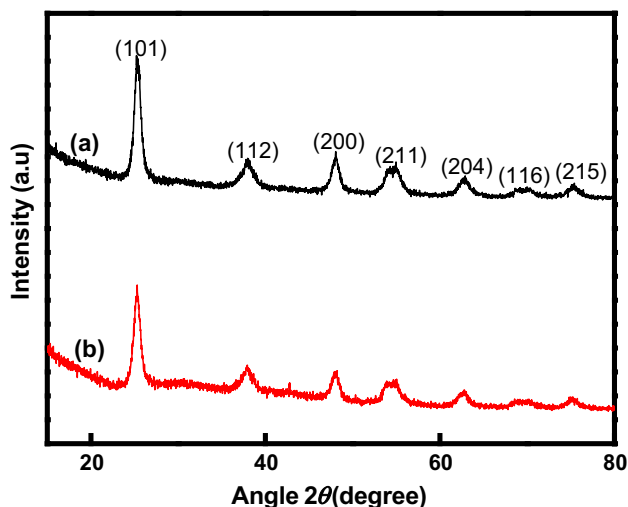


Fig. 4 XRD spectra for the **a** 1 % Ag-doped TiO₂ and **b** undoped TiO₂ annealed at 450°C

does not perturb the crystal structure of anatase TiO₂, indicating that the metal dopant is merely placed on the surface of the crystals without being covalently anchored into the crystal lattice. There are no diffraction pattern characteristics of the Ag metal in the XRD patterns.

3.1.4 Surface morphological properties

3.1.4.1 SEM and EDAX Scanning electron microscopy (SEM) was used to investigate the morphology as shown in Figs. 5a and 6a for bare and 1 % Ag-doped TiO₂, respectively. The SEM results showed the rough morphology and the presence of agglomerated nanoparticles. Bare TiO₂ particles are irregular in shape and size of approximate $20\text{ }\mu\text{m}$, whereas in the case of 1 % Ag-doped TiO₂ particles are comprised of clusters of agglomerated nanoparticles with the average particle size of about $0.5\text{ }\mu\text{m}$ ($<1\text{ }\mu\text{m}$). SEM images of Ag–TiO₂ nanoparticles confirm the presence of porous, sponge-like structure and complexity. Such structure indicates the high surface area, resulting in greater adsorption of dye, which has been proven to be useful for DSSC application. Such structure aids in the penetration of the electrolyte and expected to effectively enhance the efficiency [15]. The SEM revealed that the distribution of silver on the surface of TiO₂ is not uniform, and silver-doped TiO₂ contains irregular shaped particles, which are the aggregation of tiny crystals.

From the EDX spectra as shown in Figs. 5b and 6b, the chemical compositions of bare TiO₂ and 1 % Ag-doped TiO₂, respectively, were obtained and are given in Table 1(a, b), respectively. The characteristic peaks of Ag were observed to confirm the presence of Ag. The approximate weight percentage of Ag content was found to be approximately 1.27 %.

3.1.4.2 HRTEM HRTEM was performed for determining the sizes and morphology of the nanoparticles. HRTEM characterization of the Ag-doped TiO₂ nearly confirms the presence of Ag in TiO₂. The average particle diameter of TiO₂ and Ag-loaded TiO₂ particles was in the range $8\text{--}12\text{ nm}$ and $2\text{--}6\text{ nm}$ as shown in Figs. 7 and 8, respectively. The particles are irregular in shape but agglomerated in both cases bare and 1 % Ag-doped TiO₂.

3.1.4.3 AFM The structural effects of Ag doping leading to morphological change were studied by AFM. In Figs. 9 and 10, the AFM images of the undoped TiO₂ and 1 % Ag-doped TiO₂ are given. The three-dimensional AFM images show the nature of height mode structures and surface morphology. The estimated average rough surface measurement of the undoped TiO₂ and 1 % Ag-doped TiO₂ surface was about 7.006 and 10.588 nm , respectively. The section analysis of undoped TiO₂ and 1 % Ag-doped TiO₂

Fig. 5 **a** SEM micrograph for undoped TiO₂. **b** EDX spectra for elemental analysis of undoped TiO₂

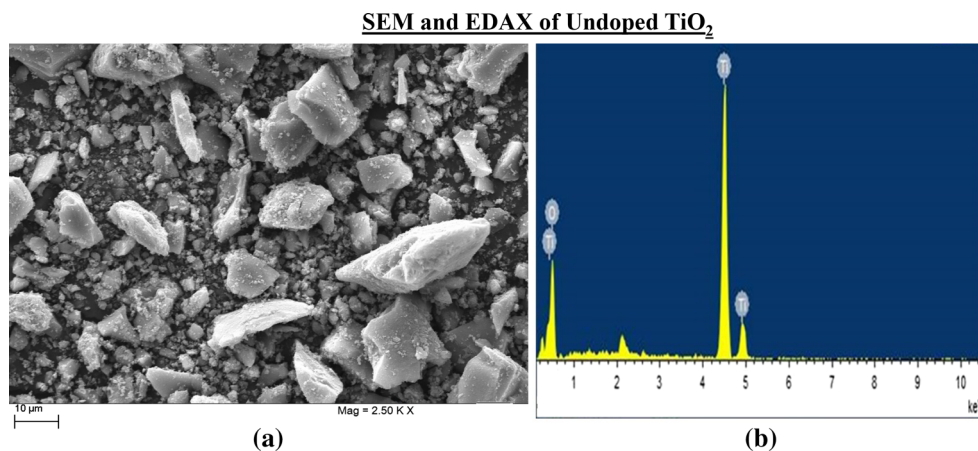


Fig. 6 **a** SEM micrograph for 1 % Ag-doped TiO₂. **b** EDX spectra for elemental analysis of 1 % Ag-doped TiO₂

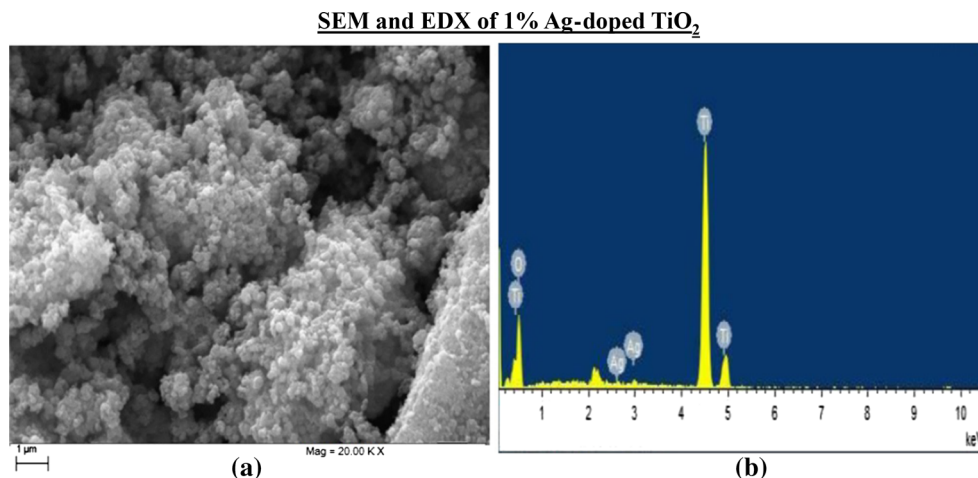


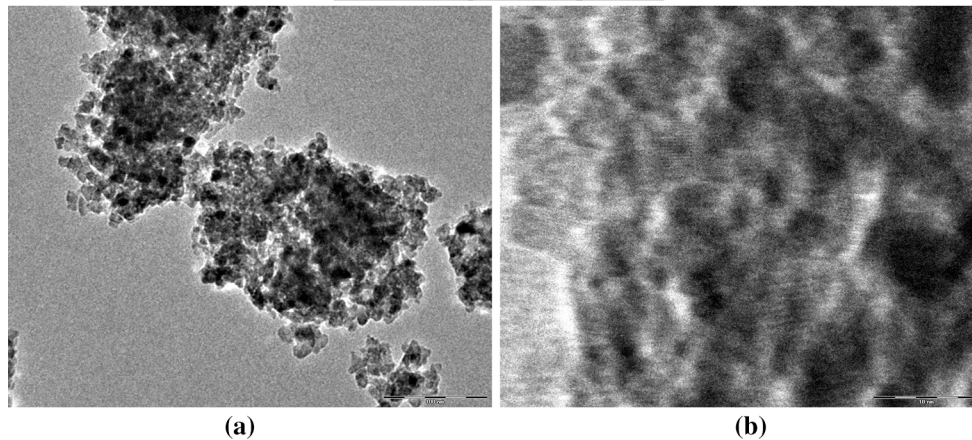
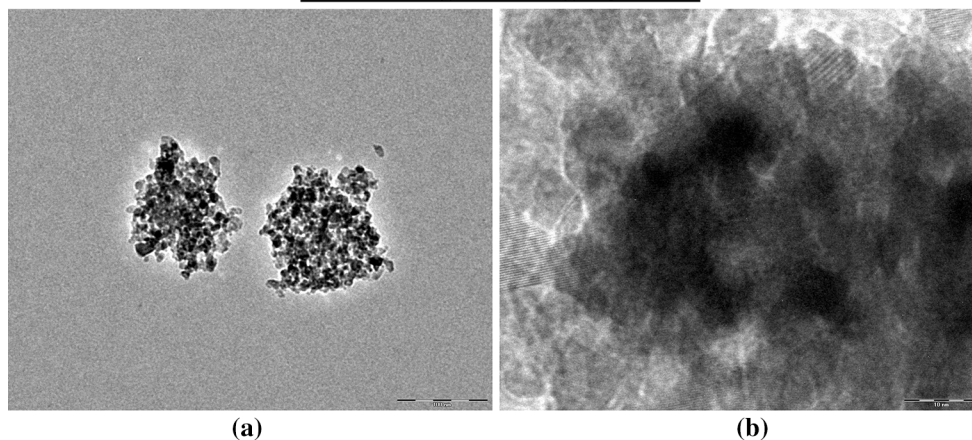
Table 1 EDAX data of (a) un-doped TiO₂, (b) 1 % Ag-doped TiO₂

Element	Weight (%)	Atomic (%)
(a)		
O–K	57.40	80.14
Ti–K	42.60	19.86
Total	100.00	100.00
(b)		
O–K	54.29	78.32
Ti–K	44.45	21.41
Ag–L	1.26	0.27
Total	100.00	100.00

surface was also done, and the morphological data obtained from AFM images of undoped and 1 % Ag-doped TiO₂ are listed in Table 2. From the study of grain analysis, average size and surface area were found to be approximately 130 nm, 0.0202 μm² and 48 nm, 0.00265 μm² for undoped TiO₂ and 1 % Ag-doped TiO₂, respectively.

3.1.5 Electrochemical impedance studies

The structural effects of the Ag doping on the kinetic behavior of dye regeneration and triiodide reduction reaction taking place at TiO₂ electrode and Pt counter electrode, respectively, were further investigated by electrochemical impedance spectroscopy measurements. Figure 11 depicts the impedance spectra of DSSC based on undoped TiO₂ and 1 % Ag-doped TiO₂ measured at OCV in the frequency range 10⁻¹–10⁵ Hz. Two semi-circles, including a small semicircle at high frequency and a large one at low frequency, were observed in the Nyquist plots of EIS spectra. The charge-transfer resistance for TiO₂/dye/electrolyte interface decreases with decreasing the semicircle diameter in the Nyquist plot. In the Bode phase plots, the frequency peak related to the 1 % Ag-doped TiO₂/FTO electrode slightly shifted to a relatively low frequency. The electron lifetime (τ_n) has been estimated from equation, $\tau_n = 1/2\pi f_{max}$, where f_{max} is peak frequency. The τ_n was found to be 1.33 and 2.05 ms for DSSC with undoped TiO₂ and 1 % Ag-doped

HRTEM Images of undoped TiO₂**Fig. 7** HRTEM spectra of un-doped TiO₂**HRTEM Images of 1% Ag-doped TiO₂****Fig. 8** HRTEM spectra of 1 % Ag-doped TiO₂

TiO₂, respectively. This enhancement in electron lifetime can contribute to an increase in the electron collection efficiency, leading to the improved J_{sc} value. The parameters obtained from the EIS studies are given in Table 3. It was observed that both R_s and R_{ct} decreased for Ag-doped TiO₂. The decrease in charge-transfer resistance R_{ct} of triiodide reduction according to the reaction given as (3) on the counter electrode gives rise to improved J_{sc} . The lower value of ohmic serial resistance R_s , which is responsible for the high ionic conductivity, may also cause the larger J_{sc} [29–31].



Therefore, the photocurrent density improvement is related to the improved carrier transport properties of the photoanode and Ag incorporation in TiO₂ increases the electrical conductivity, resulting in faster electron transport, which results in a higher photocurrent [22].

3.1.6 Photoelectrochemical studies

3.1.6.1 Current–potential curve (J – V curve) The TiO₂ powders (undoped TiO₂ and 1 % Ag-doped TiO₂) were used to make photoanodes and, after coating with N719 dye, were applied in fabricating DSSC. Figure 12i shows the photocurrent–potential (J – V) curves of such cells (dye-adsorbed TiO₂ electrode/electrolyte/platinum counter electrode) determined under illumination with light of 140 mW/cm² intensity. From the (J – V) curves, power conversion efficiency (η) and fill factors (FF) were evaluated using the following relations:

$$FF = \frac{P_{max}}{P_{ideal}} = \frac{J_{max} (A/cm^2) \times V_{max} (V)}{J_{sc} (A/cm^2) \times V_{oc} (V)} \quad (4)$$

$$\eta (\%) = \frac{J_{max} (A/cm^2) \times V_{max} (V)}{I_{inc} (W/cm^2)} \times 100 \quad (5)$$

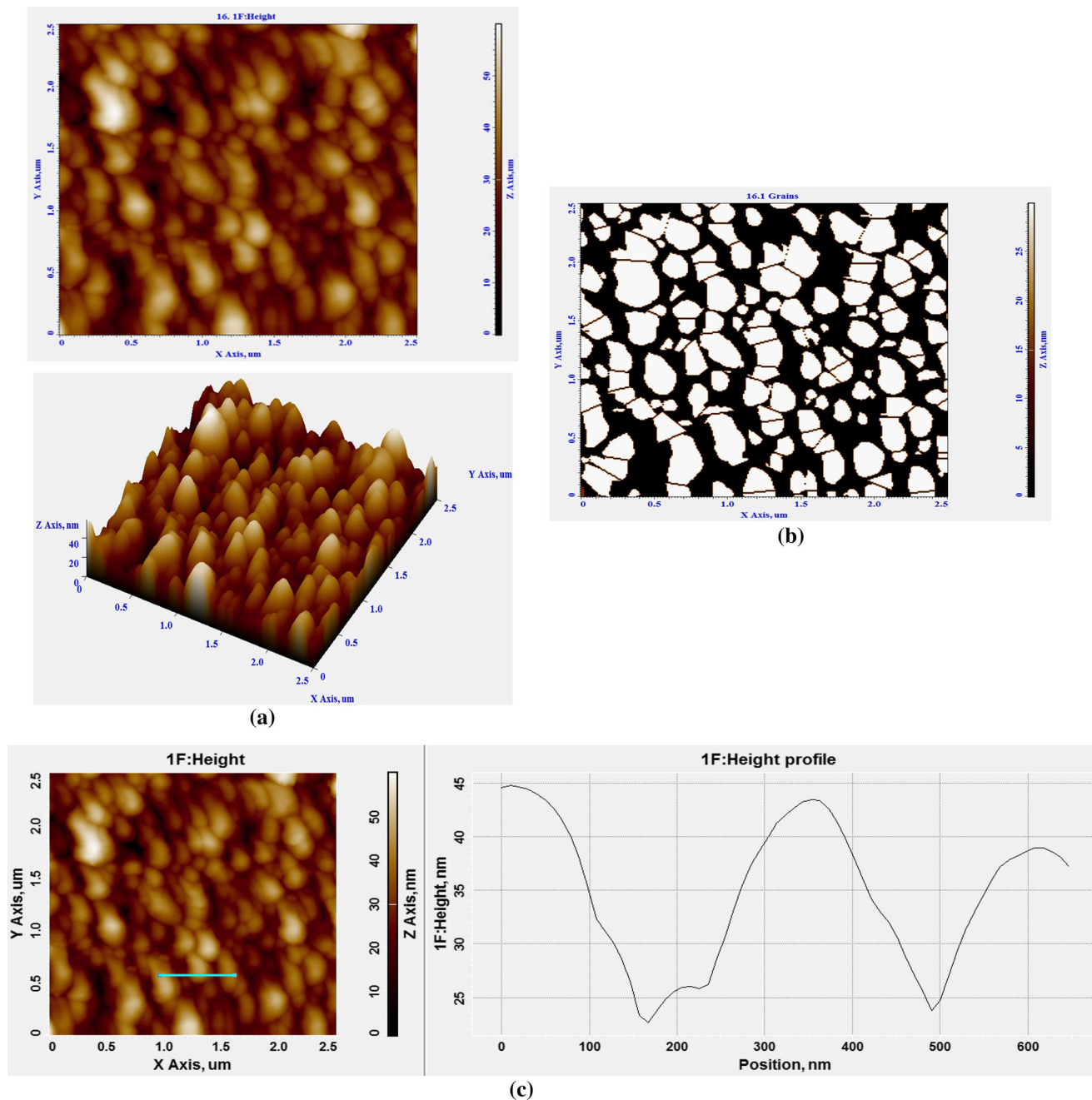


Fig. 9 **a** Two-dimensional and three-dimensional AFM images of undoped TiO₂ sintered at 450 °C. **b** AFM image for grain analysis of undoped TiO₂. **c** Topography and section analysis AFM image of undoped TiO₂ thin film (scan range 2.5 × 2.5 μm², vertical scale 60 nm)

here J_{sc} , V_{oc} and I_{inc} are short-circuit photocurrent, open-circuit potential and intensity of incident light, respectively. With Ag-doped TiO₂, J_{sc} , V_{oc} , fill factor and overall efficiency were found to be 1.07 mA cm⁻², 0.72 V, 0.73 and 0.4 %, respectively, under illumination of 140 mW cm⁻² light intensity, whereas with undoped TiO₂ under similar conditions, $J_{sc} = 0.63$ mA cm⁻², $V_{oc} = 0.70$ V, fill factor 0.45 and conversion efficiency 0.14 % could be obtained. These output parameters are

summarized in Table 3. Therefore, ~70 % increase in the photocurrent of the cell based on 1 % Ag-doped TiO₂ electrode was obtained as compared to the undoped TiO₂. The V_{oc} value of DSSC with 1 % Ag-doped TiO₂ electrode was also increased slightly. The electron lifetime of DSSC with Ag-doped TiO₂ increased from 1.33 (for undoped TiO₂) to 2.05 ms, and consequently, electron recombination was reduced. Therefore, the increased J_{sc} value in DSSC with 1 % Ag-doped TiO₂ electrode may be

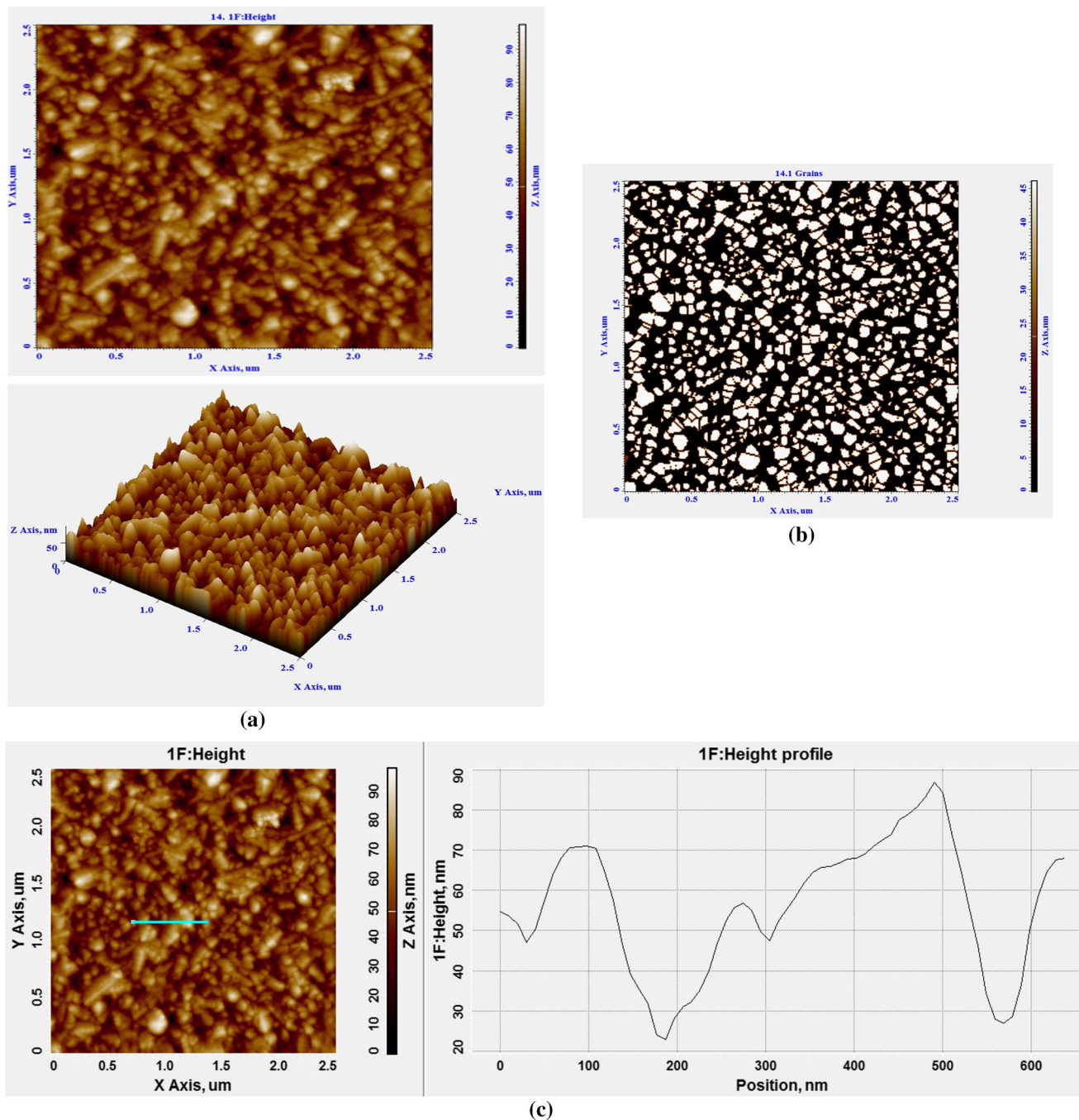


Fig. 10 **a** Two-dimensional and three-dimensional AFM images of Ag-doped TiO₂ sintered at 450 °C. **b** AFM image for grain analysis of Ag-doped TiO₂. **c** Topography and section analysis AFM image of Ag-doped TiO₂ thin film (scan range $2.5 \times 2.5 \mu\text{m}^2$, vertical scale 60 nm)

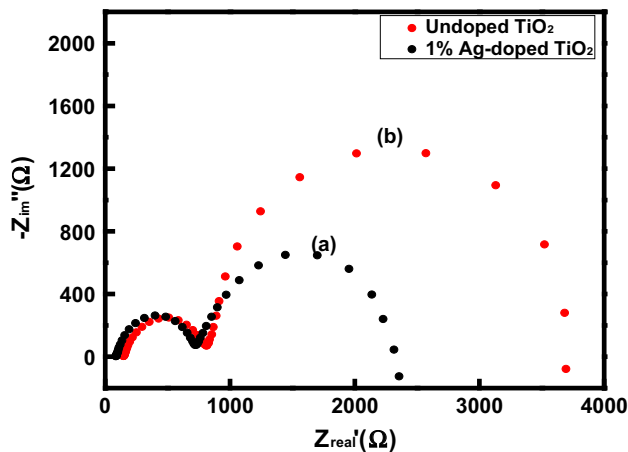
attributed to the enhancement of the dye adsorption and increased electron lifetime [32]. The increase in J_{sc} is mainly due to enhanced optical absorption of the incident photons. The enhanced J_{sc} with Ag doping implied that resistance was smaller than that of undoped TiO₂. It might be a result of the fact that the silver nanoparticles in the photoanodes shorten the electron transport pathways, allow

efficient electron transfer from the TiO₂ layer to the substrate and enhance the efficiency [21].

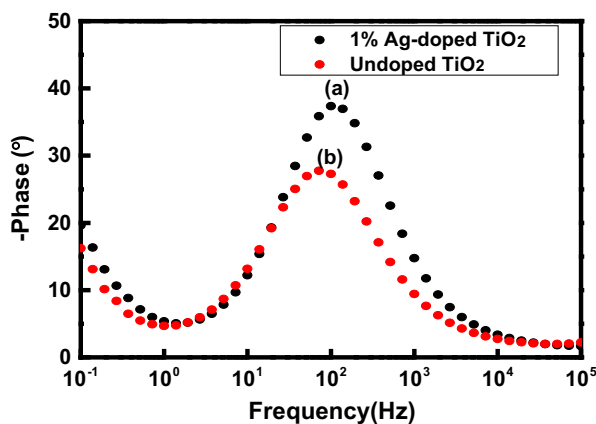
The photocurrent–potential (J – V) curves were recorded for the Ag-modified photoanodes with different Ag contents and are shown in Fig. 8ii. The observed results clearly revealed that a further increase in the Ag content eventually led to a decrease in the conversion efficiency (Fig. 8ii;

Table 2 Morphology data obtained from AFM images of undoped and 1 % Ag-doped TiO₂

TiO ₂ samples	Height parameters			Section analysis		
	Root-mean-square roughness (nm)	Average roughness (nm)	Area peak-to-valley height (nm)	Root-mean-square roughness (nm)	Average roughness (nm)	Peak-to-peak height (nm)
Undoped TiO ₂	8.744	7.006	59.876	6.6993	5.8872	22.157
1 % Ag-doped TiO ₂	13.232	10.588	97.230	16.372	13.51	64.259



(a)

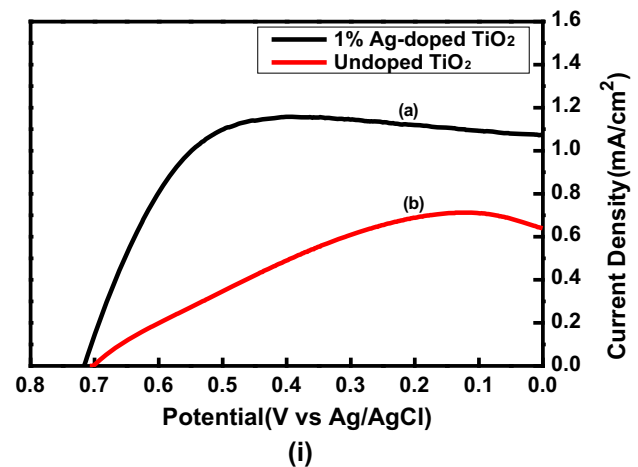


(b)

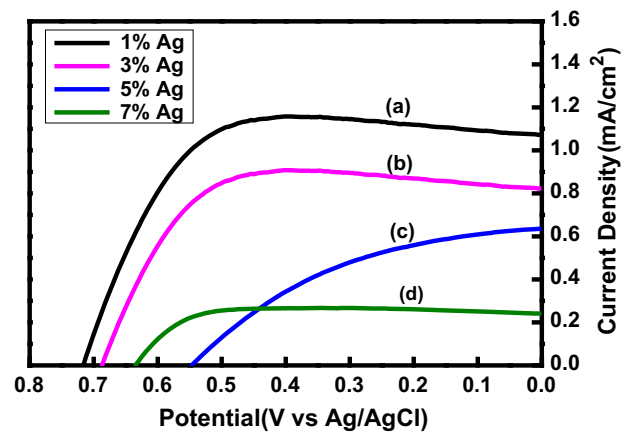
Fig. 11 Electrochemical impedance spectra showing **a** Nyquist plots and **b** Bode plots for undoped TiO₂ and 1 % Ag-doped TiO₂**Table 3** R_s , R_{ct} and τ_n of the undoped TiO₂ and 1 % Ag-doped TiO₂ films determined by electrochemical impedance spectroscopy measurement

TiO ₂ samples	R_s (Ω)	R_{ct} (k Ω)	τ_n (ms)
Undoped TiO ₂	157	2.74	1.33
1 % Ag-doped TiO ₂	92	1.47	2.05

Table 4). This is probably due to the fact that with increase in Ag concentration the active sites were shielded by large amount of Ag, leading to low carrier generation and



(i)



(ii)

Fig. 12 Photocurrent–potential curves of DSSC fabricated with. **i** 1 % Ag-doped TiO₂ and undoped TiO₂ as photoanode sensitized by N719 dye. **ii** Ag-doped TiO₂ with varied concentration of Ag (a) 1 % (b) 3 % (c) 5 % and (d) 7 %, as photoanode sensitized by N719 dye

decrease in photo performance. Moreover, when the amount of Ag loaded on the surface of TiO₂ is large, Ag becomes the recombination centre of photoelectron and hole, which leads to a decrease in the J_{sc} and V_{oc} , and consequently, the overall conversion efficiency of the DSSC gets deteriorated.

3.1.6.2 Power–potential curve The product of current density and the voltage gives the power per unit area of the

Table 4 Device performance of dye-sensitized solar cells obtained from the J – V curves shown in Fig. 12

TiO ₂ sample	J_{sc} (mA/cm ²)	V_{oc} (V)	Power (mW/cm ²)	Fill factor (%)	Efficiency (%)	IPCE (%)
Undoped TiO ₂	0.63	0.70	0.2	45	0.14	11
1 % Ag-doped TiO ₂	1.07	0.72	0.6	73	0.40	16

cell, and it takes a maximum value at a particular point on the J – V curve. The power curves were recorded for the Ag-modified photoanodes with different Ag contents and are shown in Fig. 13. The point at which the power becomes maximum is known as maximum power point (MPP), and in the present case, maximum power for 1 % Ag-doped TiO₂ and undoped TiO₂ was obtained as 0.6 and 0.2 mW/cm², respectively, which are shown in Fig. 13.

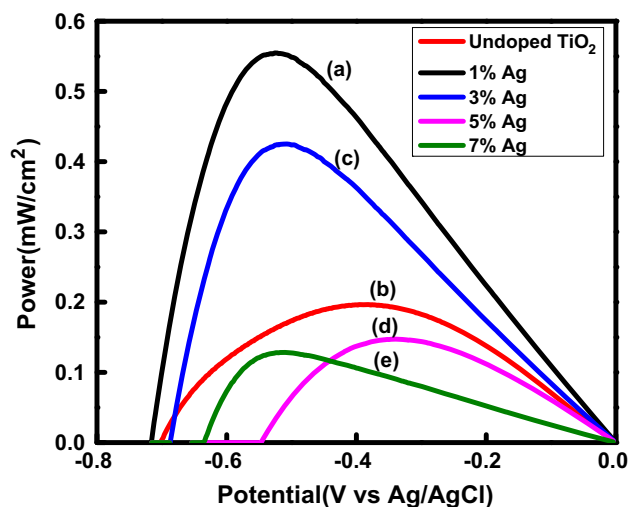
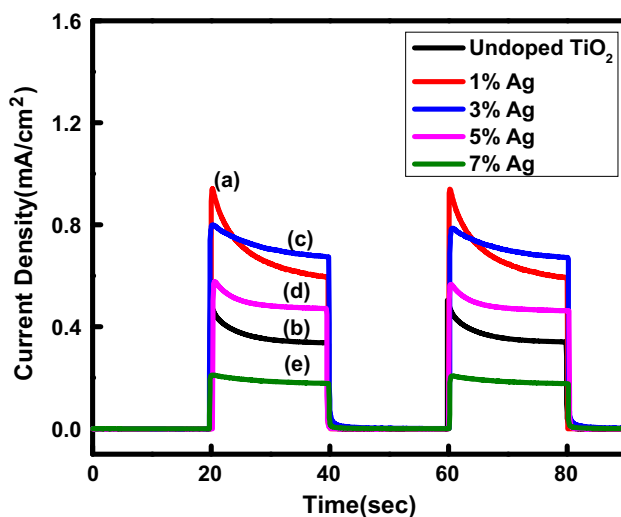
3.1.6.3 Transient photocurrent–time profile The transient current–time profiles are recorded to know the speed of the response of the photoanode to a light stimulus, and the sustainability of the photocurrent observed initially on illumination of the semiconductor electrode. For such an assessment, the time-dependent response of a dye-sensitized TiO₂ electrode to light was determined in terms of the short-circuit current, and the results for the Ag-modified photoanodes with different Ag contents are shown in Fig. 14. Somewhat greater decay was observed in case of Ag-doped TiO₂ compared to undoped TiO₂.

3.1.6.4 Action spectra (IPCE vs λ) To ascertain the sensitization of photocurrent by the dye under investigation, the action spectrum of dye-modified TiO₂ electrode was determined and is shown in Fig. 15. The short-circuit photocurrent (J_{photo}) induced by monochromatic light was determined in the 400–700 nm wavelength range. From the values of J_{sc} and the intensity of the corresponding monochromatic light (I_{inc}), the incident photon-to-current conversion efficiency (IPCE) was calculated at each excitation wavelength (λ) using following equation:

$$IPCE (\%) = \frac{1240 J_{photo} (A/cm^2)}{\lambda (nm) \times I_{inc} (W/cm^2)} \times 100 \quad (6)$$

An enhanced IPCE was obtained in case of 1 % Ag-doped TiO₂ compared to undoped TiO₂. After doping with silver, the response of TiO₂ nanoparticles to visible light was increased and showed red shift (toward longer wavelength). The red shift of the absorption curve results in a reduction of the band-gap energy and also the recombination rate and hence enhanced photoelectrochemical behavior.

3.1.6.5 Long-term stability The stability of the DSSC was assessed by measuring intermittently during 6 h the J_{sc} of two selected cells fabricated with photoanodes of

**Fig. 13** Power–potential curves of the DSSC fabricated with a 1 % Ag-doped TiO₂ and b undoped TiO₂ as photoanode sensitized by N719 dye**Fig. 14** Transient current–time curves of cell based on a 1 % Ag-doped TiO₂ and b undoped TiO₂ thin film electrode sensitized by N719 dye

undoped TiO₂ and 1 % Ag-doped TiO₂. From the results shown in Fig. 16, it was observed that during prolonged operation of the cell, the photocurrent was found to remain almost stable without any significant deterioration. Enhanced long-term stability was observed in DSSC

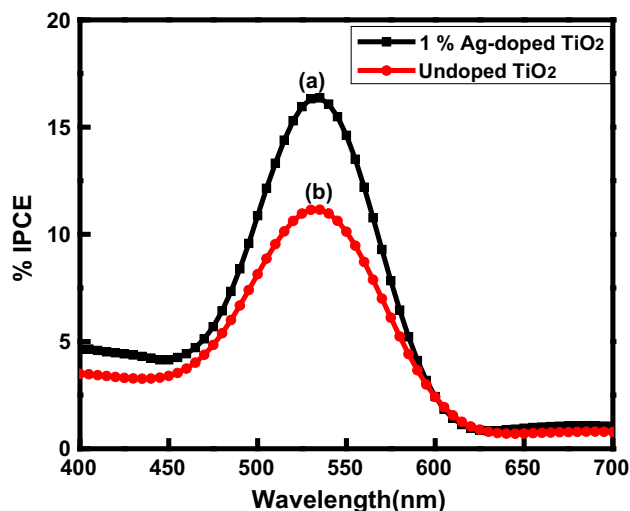


Fig. 15 Incident photon-to-current conversion efficiency (IPCE vs. λ) plots for **a** 1 % Ag-doped TiO₂ and **b** undoped TiO₂/N719/electrolyte/Pt DSSC assembly

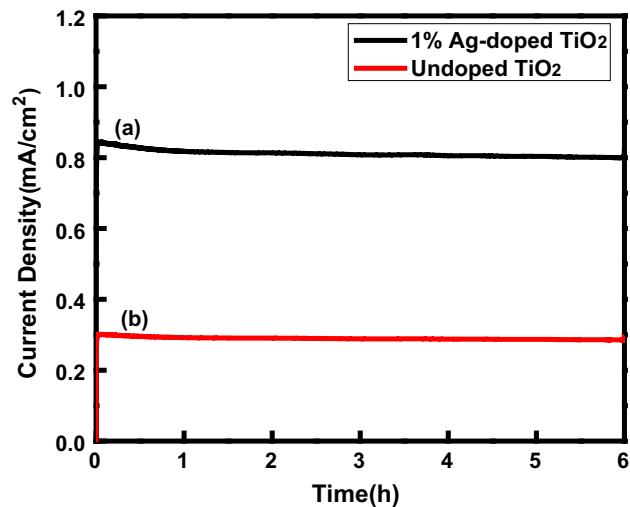


Fig. 16 Stability of photocurrent on prolonged operation (6 h) of the **a** 1 % Ag-doped and **b** undoped TiO₂/N719 based DSSC under illumination with light intensity 140 mW/cm²

containing Ag because of the strong adsorption properties. The optical band-gap energies decrease with the doping of silver ions, which allow the delay in recombination rate and enhance the photoelectrochemical behavior.

4 Conclusions

A simple approach to prepare Ag-doped TiO₂ by sol-gel method under optimized Ag content to fabricate a photoanode for DSSC was demonstrated. The properties of the as-prepared TiO₂ powders and their thin films used as

photoelectrodes in N719-sensitized solar cells were studied using UV-visible absorption, FTIR, XRD, AFM and PEC characterizations. According to XRD analysis, the prepared TiO₂ samples consisted mainly of anatase phase of titania. The optical band gap of the material was found to vary from 3.10 eV (undoped TiO₂) to 2.75 eV (Ag-doped TiO₂). Samples obtained with Ag dopant displayed differences in visible light absorption abilities due to red shifting of the band gap. The electron lifetime of DSSC with Ag-doped TiO₂ increased from 1.33 (for undoped TiO₂) to 2.05 ms. As a result of the longer τ_n , the device fabricated using Ag-doped TiO₂ showed improved J_{sc} values compared to the undoped TiO₂ photoanode-based DSSC. The characterizations suggested that greater surface coverage of the sensitizing dye with Ag-doped TiO₂ is responsible for better photovoltaic performance, and hence, improved IPCE, J_{sc} and η values were obtained.

Acknowledgments One of the authors (Arun Kumar Gupta) acknowledges the financial support received from the University Grant Commission, New Delhi, for this work.

References

1. D. Wei, Dye sensitized solar cells. *Int. J. Mol. Sci.* **11**, 1103–1113 (2010)
2. B.C. O'Regan, J.R. Durrant, Kinetic and energetic paradigms for dye-sensitized solar cells: moving from the ideal to the real. *Acc. Chem. Res.* **42**, 1799–1808 (2009)
3. A. Hagfeldt, G. Boschloo, L. Sun, L. Kloo, H. Pettersson, Dye-sensitized solar cells. *Chem. Rev.* **110**, 6595–6663 (2010)
4. M.K. Nazeeruddin, F. De Angelis, S. Fantacci, A. Selloni, G. Viscardi, P. Liska, S. Ito, B. Takeru, M. Grätzel, Combined experimental and DFT-TDDFT computational study of photoelectrochemical cell ruthenium sensitizers. *J. Am. Chem. Soc.* **127**, 16835–16847 (2005)
5. R.A. Jensen, H. Van Ryswyk, C.X. She, J.M. Szarko, L.X. Chen, J.T. Hupp, Dye-sensitized solar cells: sensitizer-dependent injection into ZnO nanotube electrodes. *Langmuir* **26**, 1401–1404 (2010)
6. H.J. Snaith, C. Ducati, SnO₂-based dye-sensitized hybrid solar cells exhibiting near unity absorbed photon-to-electron conversion efficiency. *Nano Lett.* **10**, 1259–1265 (2010)
7. K. Hara, T. Horiguchi, T. Kinoshita, K. Sayama, H. Sugihara, H. Arakawa, Highly efficient photon-to-electron conversion with mercurochrome sensitized nanoporous oxide semiconductor solar cell. *Sol. Energy Mater. Sol. Cells* **64**, 115–134 (2000)
8. S.M. Yang, H.Z. Kou, H.J. Wang, K. Cheng, J.C. Wang, Preparation and band energetics of transparent nanostructured SrTiO₃ film electrodes. *J. Phys. Chem. C* **114**, 815–819 (2010)
9. A. Fujishima, T.N. Rao, D.A. Tryk, Titanium dioxide photocatalysis. *J. Photochem. Photobiol. C* **1**, 1–21 (2000)
10. K. Pirkanniemi, M. Sillanpää, Heterogeneous water phase catalysis as an environmental application: a review. *Chemosphere* **48**, 1047–1060 (2002)
11. Y. Hu, H.L. Tsai, C.L. Huang, Effect of brookite phase on the anatase-rutile transition in titania nanoparticles. *J. Eur. Ceram. Soc.* **23**, 691–696 (2003)
12. V. Samuel, R. Pasricha, V. Ravi, Synthesis of nanocrystalline rutile. *Ceram. Int.* **31**, 555–557 (2005)

13. D. Crişan, N. Drăgan, M. Răileanu, M. Crişan, A. Ianculescu, D. Luca, A. Năstuţă, D. Mardare, Structural study of sol–gel Ag/TiO₂ films from nanopowders. *Appl. Surf. Sci.* **257**, 4227–4231 (2011)
14. B. Shanghavi, P.V. Kamat, Intersurface electron transfer in metal/semiconductor composites. Picosecond dynamics of CdS capped gold nanoclusters. *J. Phys. Chem. B* **101**, 7675–7679 (1997)
15. H. Chang, C.-H. Chen, M.-J. Kao, H.-H. Hsiao, Effect of core-shell Ag@TiO₂ volume ratio on characteristics of TiO₂-based DSSCs. *J. Nanomater.* **2014** (2014). doi:10.1155/2014/264108
16. P.-C. Huang, T.-Y. Chen, Y.-L. Wang, C.-Y. Wu, T.-L. Lin, Improving interfacial electron transfer and light harvesting in dye-sensitized solar cells by using Ag nanowire/TiO₂ nanoparticle composite films. *RSC Adv.* **5**, 70172 (2015)
17. M.A.K.L. Dissanayak, J.M.K.W. Kumari, G.K.R. Senadeera, C.A. Thotawatthage, Efficiency enhancement in plasmonic dye-sensitized solar cells with TiO₂ photoanodes incorporating gold and silver nanoparticles. *J. Appl. Electrochem.* **46**, 47–58 (2016)
18. Y. Liu, G. She, X. Qi, L. Mu, X. Wang, W. Shi, Contributions of Ag nanowires to the photoelectric conversion efficiency enhancement of TiO₂ dye-sensitized solar cells. *J. Nanosci. Nanotechnol.* **15**(6), 7068–7073 (2015)
19. E.M. Jin, X.G. Zhao, J.-Y. Park, Gu H-B, Enhancement of the photoelectric performance of dye-sensitized solar cells using Ag-doped TiO₂ nanofibers in a TiO₂ film as electrode. *Nanoscale Res. Lett.* **7**, 97 (2012)
20. H.-H. Huang, H. Chang, H.-W. Liu, C.-W. Hsu, C. Chiu, M.-Y. Teng, H.-J. Lai, I.-C. Cheng, J.-Z. Chen, Plasma-etched nanoporous TiO₂ using Ag nanoparticle masks: application for photoanodes of dye-sensitized solar cells. *Mater. Res. Express* **1**, 025505 (2014)
21. A. Ranjitha, N. Muthukumarasamy, M. Thambidurai, D. Velauthapillai, Enhanced photovoltaic performance of quantum dot sensitized solar cells with Ag-doped TiO₂ nanocrystalline thin films. *J. Mater. Sci. Mater. Electron.* **25**, 2724–2729 (2014)
22. J. Li, X. Chen, N. Ai, J. Hao, Q. Chen, S. Strauf, Y. Shi, Silver nanoparticle doped TiO₂ nanofiber dye sensitized solar cells. *Chem. Phys. Lett.* **514**, 141–145 (2011)
23. D.J.R. Gutiérrez, N.R. Mathews, S.S. Martínez, Photocatalytic activity enhancement of TiO₂ thin films with silver doping under visible light. *J. Photochem. Photobiol. A* **262**, 57–63 (2013)
24. X. Houa, H. Maa, F. Liua, J. Denga, Y. Aia, X. Zhaoa, D. Maoa, D. Lia, B. Liaoba, Synthesis of Ag ion-implanted TiO₂ thin films for antibacterial application and photocatalytic performance. *J. Hazard. Mater.* **299**, 59–66 (2015)
25. G. Yang, Z. Jiang, H. Shi, T. Xiao, Z. Yan, Preparation of highly visible-light active N-doped TiO₂ photocatalyst. *J. Mater. Chem.* **20**, 5301–5309 (2010)
26. J. Geng, D. Yang, J. Zhu, D. Chen, Z. Jiang, Nitrogen-doped TiO₂ nanotubes with enhanced photocatalytic activity synthesized by a facile wet chemistry method. *Mater. Res. Bull.* **44**, 146–150 (2009)
27. H.K. Park, D.K. Kim, C. Hee, Effect of solvent on titania particle formation and morphology in thermal hydrolysis of TiCl₄. *J. Am. Ceram. Soc.* **80**, 743–749 (1997)
28. K. Yeung, S.T. Yau, A.J. Maira, J.M. Coronado, J. Soria, P.L. Yue, The influence of surface properties on the photocatalytic activity of nanostructured TiO₂. *J. Catal.* **219**, 107–116 (2003)
29. Q. Zheng, H. Kang, J. Yun, J. Lee, J.H. Park, S. Baik, Hierarchical construction of self-standing anodized titania nanotube arrays and nanoparticles for efficient and cost-effective front-illuminated dye-sensitized solar cells. *ACS Nano* **5**, 5088–5093 (2011)
30. J. Bisquert, I.N. Mora-Sero, Simulation of steady-state characteristics of dye-sensitized solar cells and the interpretation of the diffusion length. *J. Phys. Chem. Lett.* **1**, 450–456 (2009)
31. J. Bisquert, Chemical capacitance of nanostructured semiconductors: its origin and significance for nanocomposite solar cells. *J. Phys. Chem. Chem. Phys.* **5**, 5360–5364 (2003)
32. A.R. Andersen, J. Halme, T. Lund, M.I. Asghar, P.T. Nguyen, K. Miettunen, E. Kemppainen, O. Albrechtsen, Charge transport and photocurrent generation characteristics in dye solar cells containing thermally degraded N719 dye molecules. *J. Phys. Chem. C* **115**, 15598–15606 (2007)